Effects of quantum noise on the nonlinear dynamics of a semiconductor laser subject to two spectrally filtered, time-delayed optical feedbacks

Joseph S. Suelzer[a,*], Awadhesh Prasad[b], Rupamanjari Ghosh[c], Gautam Vemuri[a]

[a] *Department of Physics, Indiana University Purdue University Indianapolis (IUPUI) Indianapolis, IN 46202-3273*
[b] *Department of Physics and Astronomy, University of Delhi, Delhi 110007, India*
[c] *Shiv Nadar University, NH-91, Tehsil Dadri, Gautam Buddha Nagar, UP 201314, India*

Abstract

We report on a theoretical and computational investigation of the complex dynamics that arise in a semiconductor laser that is subject to two external, time-delayed, filtered optical feedbacks with special attention to the effect of quantum noise. In particular, we focus on the dynamics of the instantaneous optical frequency (wavelength) and its behavior for a wide range of feedback strengths and filter parameters. In the case of two intermediate filter bandwidths, the most significant results are that in the presence of noise, the feedback strengths required for the onset of chaos in a period doubling route are higher than in the absence of noise. We find that the inclusion of noise changes the dominant frequency of the wavelength oscillations, and that certain attractors do not survive in the presence of noise for a range of filter parameters. The results are interpreted by use of a combination of phase portraits, rf spectra, and first return maps.

Keywords: `elsarticle.cls`, LaTeX, Elsevier, template
2010 MSC: 00-01, 99-00

1. Introduction

A semiconductor laser (SCL) subject to feedback has become a paradigm for studying nonlinear dynamics in time-delayed feedback systems. At a fundamental level, studies on such systems are an ideal test bed for delay systems, and at an applied level, some of the dynamical behaviors have been exploited for cryptography, random-bit generation and even understanding of collective neuronal excitations in the brain [1, 2, (see references therein)]. A number of impressive studies on electronic feedback and all-optical feedback, and the resulting dynamics in a SCL have been reported over the years [3, 4]. Within the context of all-optical feedback, investigators have studied conventional optical feedback where a mirror is placed in front of the SCL such that a fraction of the light from the laser is reflected back into it [5, 6]. Other feedback scenarios have included polarization rotated feedback where the polarization of the feedback light is rotated relative to the dominant polarization mode of the laser light [7, 8, 9]. Recently, the effects of injection on the stability properties from two polarization modes has been studied [10].

Another interesting feedback scheme that has been reported is filtered optical feedback (FOF) wherein the feedback light is spectrally filtered before entering the laser [11]. FOF provides the user with two additional parameters, the bandwidth of the filter and the detuning between the filter frequency and the laser light frequency, to control the dynamics of the laser. One of the major dynamical effects observed in FOF is that the frequency of the laser light, for a judicious choice of filter parameters, exhibits controlled oscillations at a frequency that is related to the time delay of the feedback [12]. It has also been shown that for other filter parameters, one can observe a period doubling route to chaos in the frequency of the laser light [13].

Recently, there has been an interest in the dynamics of a SCL subject to two simultaneous FOFs [14, 15]. Krauskopf and co-workers have reported an exhaustive study of the bifurcations that arise in such systems [16, 17]. The use of two filters provides a number of additional parameters that can be potentially used to control the dynamics of the SCL. Our group reported an experimental study on the frequency dynamics in the light from the laser when subject to two FOFs [18]. Among the more interesting observations was the generation of new frequencies in the system, and the results were explained via a theoretical model that consisted of the usual Lang-Kobayashi rate equations augmented to include two FOFs. The agreement between experiments and theory was excellent.

One of the observations that emerged from our prior work was that the frequency of laser light in a SCL subject to two FOFs follows a period-doubling route to chaos. However, the feedback strength necessary for coherence collapse that was predicted by the theoretical model was higher than what was observed experimentally. This mis-

*Corresponding author
Email address: `josesuel@iupui.edu` (Joseph S. Suelzer)

This is the author's manuscript of the article published in final edited form as: Suelzer, J. S., Prasad, A., Ghosh, R., & Vemuri, G. (2016). Effects of quantum noise on the nonlinear dynamics of a semiconductor laser subject to two spectrally filtered, time-delayed optical feedbacks. Optics Communications, 370, 209–221. http://doi.org/10.1016/j.optcom.2016.03.017

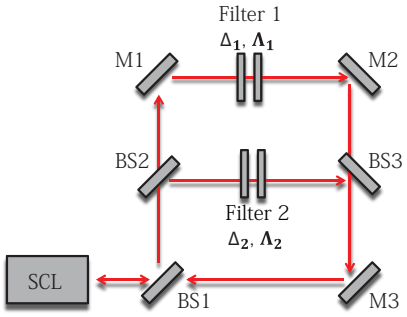

Figure 1: The schematic shows a semiconductor laser (SCL) subject to optical feedback from two external cavities. The outer cavity (1) is formed by the SCL and the mirrors (M1, M2, and M3). The inner cavity (2) is formed by the SCL, beam splitters (BS2 and BS3), and mirror (M3). Each cavity contains a Fabry-Perot resonator acting as a spectral filter, which can be modified by changing the reflectivity or spacing of the filter mirrors. This in turn changes the bandwidth, Λ. The detuning, Δ, is altered by adjusting the pump current. The delay-times, τ_1 and τ_2, are increased or decreased by lengthening or shortening the cavities.

match between theory and experiment inspired us to examine the role of unavoidable quantum noise in the laser and its influence on the dynamics of the laser. To this end, we have augmented the theoretical model with Langevin noise terms to account for the spontaneous emission noise as well as inversion noise. To give one a picture of the system studied, we show a schematic of the experimental design [Fig.1] highlighting the key parameters accessible to experiment, which are detailed in the following section.

2. Model

A semiconductor laser with FOF from a single cavity can be modeled with a set of rate equations describing the time evolution of the slowly varying complex electric fields, $E(t)$ and $F(t)$, of the laser and feedback field, respectively, and the carrier inversion $N(t)$ [11]. Our setup [Fig. 1], which includes two cavities, each with a spectral filter, must therefore include two filtered feedback fields, $F_1(t)$ and $F_2(t)$, resulting in the following description,

$$\frac{dE}{dt} = \frac{1}{2}(1+i\alpha)\xi N(t)E(t) + \kappa_1 F_1(t,\tau_1) + \kappa_2 F_2(t,\tau_2) + L_E(t), \tag{1a}$$

$$\frac{dN}{dt} = J - J_{thr} - \frac{N(t)}{T_1} - [\Gamma_0 + \xi N(t)]|E(t)|^2 + L_N(t), \tag{1b}$$

$$\frac{dF_1}{dt} = \Lambda_1 E(t-\tau_1)\mathrm{e}^{-i\omega_0\tau_1} + (i\Delta_1 - \Lambda_1)F_1(t). \tag{1c}$$

$$\frac{dF_2}{dt} = \Lambda_2 E(t-\tau_2)\mathrm{e}^{-i\omega_0\tau_2} + (i\Delta_2 - \Lambda_2)F_2(t), \tag{1d}$$

where ξNE in the first term of Eq. (1a) accounts for the growth (or decay) when the carrier inversion $N(t)$ is above (or below) threshold, and ξ is the differential gain coefficient. α is the linewidth enhancement factor which quantifies the phase-amplitude coupling. The second (third) term in Eq. (1a) accounts for the feedback field $F_1(t,\tau_1)$ ($F_2(t,\tau_2)$), where κ_1 (κ_2) is the feedback rate and τ_1 (τ_2) is the time delay due to the propagation of the feedback field in cavity 1 (2).

The rate equation for the carrier inversion [Eq. (1b)] depends on the difference between the pump current J and the threshold current J_{thr}. The second term [Eq. (1b)] accounts for the spontaneous decay, hence T_1 is the carrier decay rate, and the third term includes the stimulated emission, where Γ_0 is the photon decay rate.

Eqs. (1c) and (1d) are derived by assuming that the response function, $r(\omega)$, of the filter is Lorentzian [11], i.e.

$$r(\omega) = \frac{\Lambda}{\Lambda + i(\omega - \Delta)}, \tag{2}$$

where ω is the instantaneous optical frequency, Λ is the half width at half maximum (HWHM) of the filter and Δ is the detuning of the solitary laser frequency from the center frequency of the filter. The explicit dependence on the time-delayed fields $E(t-\tau_{1,2})$ is seen in Eqs.(1c) and (1d). The feedback phase accumulated due to the propagation of the field through cavity 1 (2) is given by $\omega_0\tau_1$ ($\omega_0\tau_2$), which we assume equal for the two cavities and fix at $\omega_0\tau_1 = \omega_0\tau_2 \equiv \theta$. The spontaneous-recombination noise terms are described by $L_E(t)$ and $L_N(t)$. Both noise sources are assumed to be Gaussian with zero mean. Their autocorrelation functions are given by,

$$\langle Re(L_E(t))Im(L_E(t'))\rangle = 0, \tag{3a}$$

$$\langle Re(L_E(t))Re(L_E(t'))\rangle = \langle Im(L_E(t))Im(L_E(t'))\rangle = R_{sp}\delta(t-t'), \tag{3b}$$

$$\langle L_N(t)L_N(t')\rangle = D\delta(t-t'). \tag{3c}$$

The rate of spontaneous emission is written as $R_{sp} = \beta_{sp}CN^2$, where β_{sp} is the fraction of spontaneous emission coupled into the dominant mode and C is a radiative recombination rate [19]. The shot noise diffusion rate is given by D. The noise sources L_E and L_N are derived quantum mechanically in order to arrive at their explicit form and statistical properties [20]. Although the noise sources are correlated in a SCL [20], we found that correlating sources resulted in no significant difference when compared to uncorrelated noise [21]. Therefore, the proceeding analysis is done with uncorrelated noise.

Eqs. (1) are integrated using a modified fourth order Runge-Kutta method. The time step was varied from 0.1 ps to 10 ps in order to ensure consistent dynamical behavior independent of the integration step size. The modified Runge-Kutta method accounts for the Langevin noise source and avoids an infinite variance of the stochastic terms following the stochastic Runge-Kutta algorithm outlined in Ref. [22]. At each integration step, the noise terms

are pulled from a matrix of normally distributed random numbers generated via the *randn()* function in MATLAB. In order to account for the time delayed fields, a history function is built by initially integrating Eqs. (1) without feedback ($\kappa_{1,2} = 0$). The transient behavior is discarded and the history function with a minimum integration time of $4\tau_{1,2}$ is saved. The remaining parameters and noise strengths for a typical edge emitting SCL are highlighted in Table 1.

Table 1: The parameter values for a typical SCL which are used in the simulations (unless otherwise specified).

Quantity	Symbol	Value
Linewidth enhancement factor	α	5
Feedback rate field 1	κ_1	Varies
Feedback rate field 2	κ_2	0.8 GHz
Bandwidth of filter 1	Λ_1	Varies
Detuning of filter 1	Δ_1	Varies
Bandwidth of filter 2	Λ_2	1.0 GHz
Detuning of filter 2	Δ_2	-1.5 GHz
Delay-time field 1	τ_1	14.28 ns
Delay-time field 2	τ_2	7.93 ns
Phase accumulation	θ	1.111
Differential gain coefficient	ξ	5×10^3 s^{-1}
Photon decay rate	Γ_0	10^{11} s^{-1}
Carrier decay rate	T_1	1 ns
Threshold pump rate	J_{thr}	1×10^{17} s^{-1}
Pump rate	J	$1.5J_{thr}$
Spontaneous emission rate	R_{sp}	5×10^{12} s^{-1}
Shot noise diffusion rate	D	1.45×10^{16} s^{-1}

We point out that this system contains a rich variety of parameters that are accessible in an experiment. Adjusting the pump current J controls the optical frequency, which in turn changes the detuning $\Delta_{1,2}$. Changing the filter mirror spacing or reflectivity modifies the bandwidth $\Lambda_{1,2}$, and the time delays $\tau_{1,2}$ are directly proportional to the external cavity lengths $L_{1,2}$. The feedback rates $\kappa_{1,2}$ are controlled via a neutral density filter inserted in each cavity.

3. Results: a period doubling route to chaos

This section describes the results of our work, but before doing so it is important to point out that the 2FOF system has a large set of parameters, each of which can influence the resulting dynamics. We have, therefore, focused on a limited set which highlights the role of quantum noise. For example, we have chosen typical noise strengths and have not varied the strength of the noise. Furthermore, we have fixed the bandwidth of one of the filters to 1GHz, the so-called intermediate bandwidth which lies between the external cavity mode spacing frequency and the laser relaxation oscillation (RO) frequency, and varied the bandwidth of the second filter to study the effects of filter bandwidth.

We begin by describing the results of our calculations, shown in Fig. 2, which exhibits a period doubling route to chaos of the frequency $\omega(t)$ of the laser wavelength (instantaneous frequency) oscillations. The period doubling route is produced via the bifurcation parameter κ_1, which is the feedback rate of field 1. The color scheme corresponds to the amplitude of the oscillations. All other parameters are fixed as specified in Table 1 except the filter bandwidth and detuning, where $\Lambda_1 = 1$ GHz and $\Delta_1 = -0.5$ GHz. Initially the feedback is solely from cavity 2 ($\kappa_2 = 0.8$ GHz and $\kappa_1 = 0$ GHz). We calculate the time series for $E(t)$, $F_{1,2}(t)$, and $N(t)$. Using the complex electric field $E(t)$ we extract the phase $\phi(t)$, where $\phi(t) = arg(E(t))$. $arg(z)$ is the typically defined complex argument of z. The frequency $\omega(t)$ of the slowly varying complex electric field $E(t)$ is found by calculating the time derivative of the phase [$\omega(t) = \dot{\phi}(t)$]. Finally, the numerical spectra are determined for $E(t)$ and $\omega(t)$ after discarding the transient behavior. The feedback rate κ_1 is increased by $\Delta\kappa_1 \approx 0.32$ GHz and this process is repeated over 32 iterations in order to arrive at a final feedback rate of $\kappa_1 = 10$ GHz. In the presence of noise, this procedure is averaged over 1000 instances. These spectra are stitched together resulting in a period doubling route to chaos shown in Fig. 2. Examining the deterministic period doubling map [Fig. 2a], the first frequency (labeled f_I) to emerge is 105 MHz corresponding to the fundamental frequency from cavity 2 ($f_2 \approx \frac{1}{\tau_2 + 1/\Lambda_2} \approx 107$ MHz). Note that the fundamental frequency, which we label as f_{fun}, for FOF is dependent on both the delay time τ and the bandwidth Λ. κ_1 is increased and a frequency (f_{II}) of 130 MHz is produced which corresponds to an average between the fundamental frequency of cavity 2 and the second harmonic of cavity 1 ($\frac{f_2 + 2f_1}{2} \approx 125$ MHz). A further increase in κ_1 results in a quasi period-doubling route to chaos. Examining the deterministic case in Fig. 2a, it is clear that the onset of chaos begins at $\kappa_1 \approx 4.5$ GHz. When noise is present, shown in Fig. 2b, the period doubling route for smaller frequencies is drastically altered. The onset of chaos is delayed and a spread in the spectrum does not emerge until $\kappa_1 \approx 7$ GHz. Not only is the chaotic regime shifted to a larger feedback rate, but the frequency content is altered. The stochastic spectra, which are extended to 5 GHz and shown in Fig. 2c, also depict a change near $\kappa_1 \approx 4.5$ GHz. The deterministic spectra (not shown) are very similar when depicted on the same scale. One gains an insight into the mechanism for this delay by examining the dynamics at different parameters in more detail.

3.1. Influence of noise

Previous studies of a SCL subject to FOF demonstrated that noise influences the dynamics substantially [21, 23]. They showed that multiple attractors exist for the deterministic dynamics, and in the presence of noise some of the attractors no longer survive [21]. The argument followed that noise helps determine whether a particular attractor

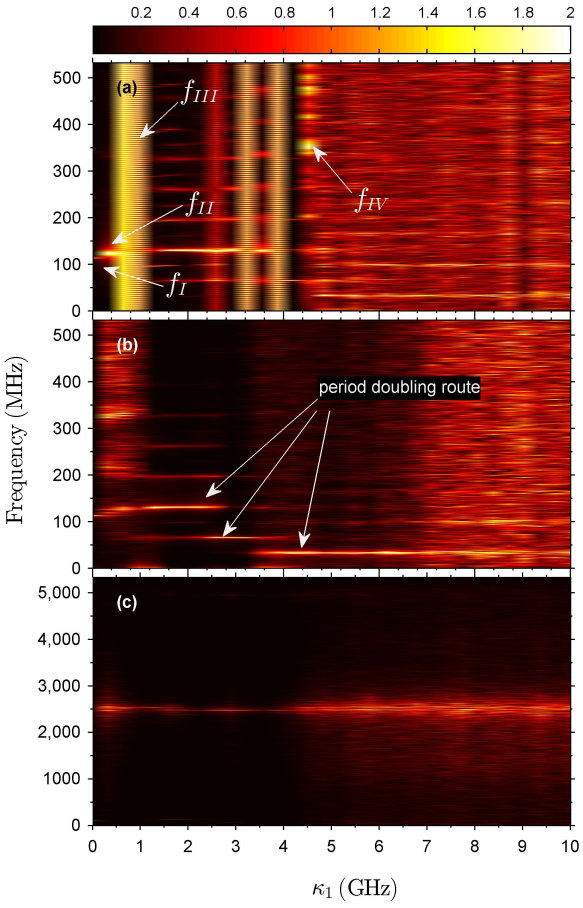

Figure 2: Deterministic (a) and stochastic [(b),(c)] density plots of the period doubling route to chaos when the feedback strength κ_1 from cavity 1 is increased. The bandwidth and detuning are fixed at $\Lambda_1 = 1$ GHz and $\Delta = -0.5$ GHz, otherwise all other parameters are recorded in Table 1. f_{I-IV} are the frequencies discussed in this text which differ significantly in the stochastic period doubling route. Note that (c) contains the stochastic spectra extended out to 5 GHz.

is stable, analogous to that of a perturbation acting on a system at a maximum of a potential distribution. Other studies have shown that noise induces jumps between stable attractors if the ratio of the noise strength to potential barrier is large enough [23]. A good understanding of this behavior is gained via an examination of the time-series in conjunction with the phase-portraits and rf spectra. The previous studies investigated particular instances of a parameter space, while we focus on the period-doubling route to chaos as the feedback strength is increased. Using these tools with the addition of first return maps, the period doubling route is traced along increasing feedback strength κ_1. The return map is generated by determining the maximum values (ω_{max}) for each oscillation in the time series $\omega(t)$. Thus a series of maximum values is generated, and $\omega_{(max)\,n+1}$ is compared to the previous value at $\omega_{(max)\,n}$.

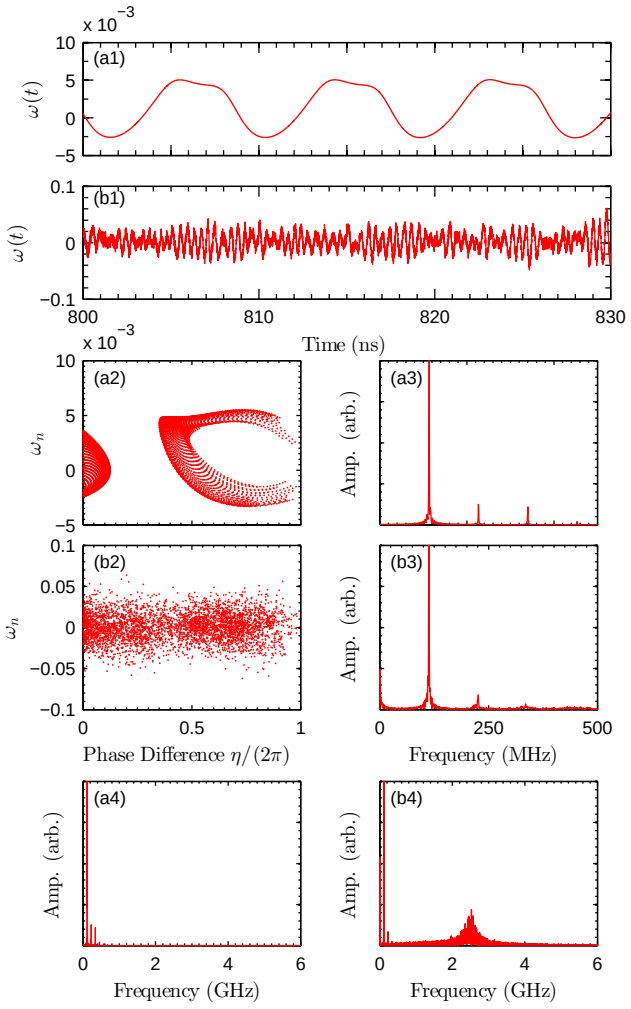

Figure 3: Deterministic (a) and stochastic (b) plots of the frequency $\omega(t)$ time-series (1), the phase-plane of ω_n and η (2), and the rf spectrum (3) showing a fundamental frequency of $f_{fun} \approx 123$ GHz. The plots are calculated when the feedback is injected solely from cavity 2 ($\kappa_1 = 0$ GHz). The rf spectra (a4) and (b4) are extended out to 6 GHz in order to depict the undamping of the ROs seen in the time-series (b1).

Fig. 3 depicts four deterministic plots and four stochastic plots. When the feedback strength is $\kappa_1 = 0$ GHz, the three corresponding plots are the instantaneous frequency $\omega(t)$ time series (a1 and b1), the phase plane of the frequency ω_n and phase difference $\eta = \phi(t) - \phi(t-\tau)$ (a2 and b2), and the rf spectrum of $\omega(t)$ (a3 and b3). We note, when comparing the deterministic (a3) and stochastic (b3) rf spectra, that the perturbation of noise does not affect the dominant frequencies in time-delay regime, even though the time-series are clearly different. This difference is noted in the large rf spectra (a4 and b4), where in the presence of noise (b4) the ROs are undamped. However, as we increase the feedback strength κ_1, noise plays a significant role in determining the dominant frequencies.

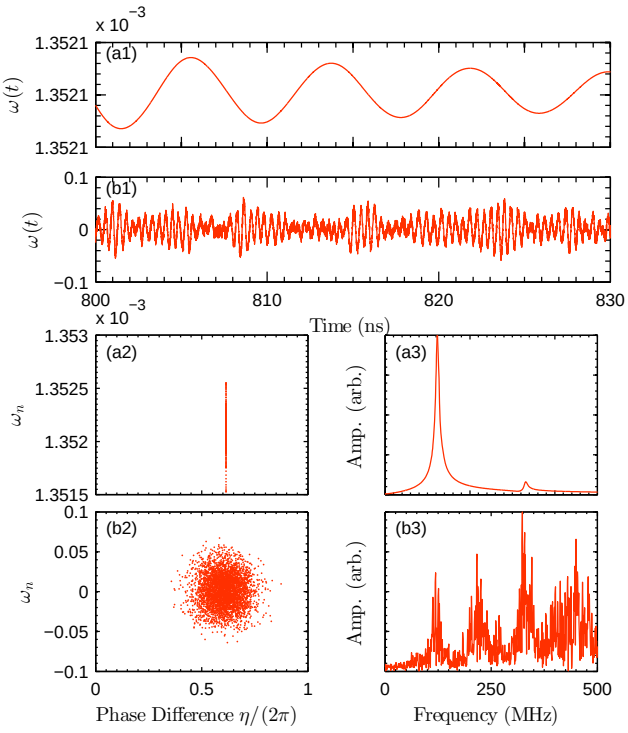

Figure 4: Deterministic (a) and stochastic (b) plots of the frequency $\omega(t)$ time-series (1), the phase-plane of ω_n and η (2), and the RIN spectrum (3) when the feedback strength is κ_1 =0.32 GHz. The deterministic time-series captures a transient behavior toward a steady-state behavior.

Once the feedback from the first cavity is allowed ($\kappa_1 = 0.32$ GHz), as shown in Fig. 4, the deterministic and stochastic rf spectra [(a3) and (b3)] show clear differences. The differences can be understood by examining the deterministic and stochastic time series [(a1) and (b1)] and phase portraits [(a2) and (b2)]. From the time series (a1), it is clear that the frequency $\omega(t)$ is always positive and $\omega(t)$ evolves toward a steady-state. The movement toward a steady state (fixed point) is depicted in the deterministic phase portrait (a2). The dominant frequency in the deterministic spectrum (a3) is ~ 125 MHz. In the presence of noise (b3), the peak at ~ 125 MHz is reduced and the peak at ~ 337 MHz is enhanced. In addition, the frequency, shown in the stochastic time series (b1), oscillates around $\omega = 0$. We note that this shift in the frequency toward $\omega = 0$ is a general feature when noise is included in the simulations. For this feedback strength ($\kappa = 0.32$ GHz), the shift occurs because the fixed point no longer survives in the presence of noise. The absence of the fixed point is clearly depicted when one compares the deterministic and stochastic return maps, shown in Fig. 5. Examining the return map (Fig. 5), the deterministic maxima (blue circles) show little variance and are centered at the fixed point, while the stochastic maxima (red triangle) spread and are no longer centered at the same location. Instead, noise drives the system toward higher frequencies coinciding with higher harmonics shown in the rf spectrum of Fig. 4(b3).

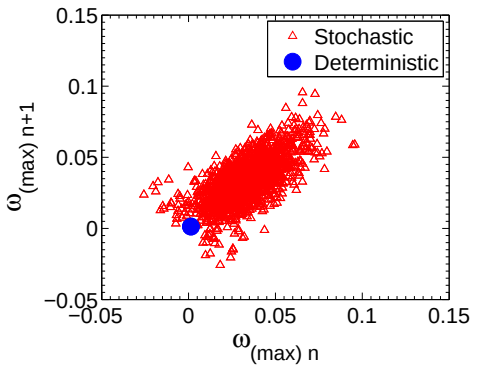

Figure 5: First return maps for feedback strength of κ_1 =0.32 GHz showing both the stochastic (red triangle) and deterministic (blue circle) locations of ω_{max}.

At a feedback strength of $\kappa_1 = 0.97$ GHz, the time-series in Fig. 6 shows periodic oscillations with a period of $1/f_{RO} = 400$ ps, where f_{RO} is the frequency of the ROs. This behavior corresponds to the undamping of the ROs, which then become the dominant feature. This undamping of the ROs is a well studied phenomenon of a SCL subject to optical feedback, where the ROs are an exchange of energy between the photons and the inversion carriers when the SCL is externally perturbed [24]. The frequency of these oscillations occur near $f_{RO} \approx 2.5$ GHz and varies depending on the SCL design and parameters. The phase portrait [Fig. 6(a2)] shows a periodic attractor, which does not survive in the presence of noise [Fig. 6(b2)]. The extinction of this attractor allows the time-delay oscillations to influence the global behavior seen in the stochastic rf spectrum [Fig. 6(b3)].

Signatures of the ROs in the dynamics occur at three instances along the bifurcation map of Fig. 2(a) at $\kappa_1 = 0.97$ GHz (f_{III} on the map), $\kappa_1 = 3.1$ GHz, and $\kappa_1 = 3.5$ GHz. Each instance displays the same behavior characterized by frequency oscillations with a period of $1/f_{RO} = 400$ ps and the existence of a limit cycle in the phase-portrait. However, in each case, this attractor no longer survives in the presence of noise. Noise drives the system toward periodic oscillations which are dictated by the delay time

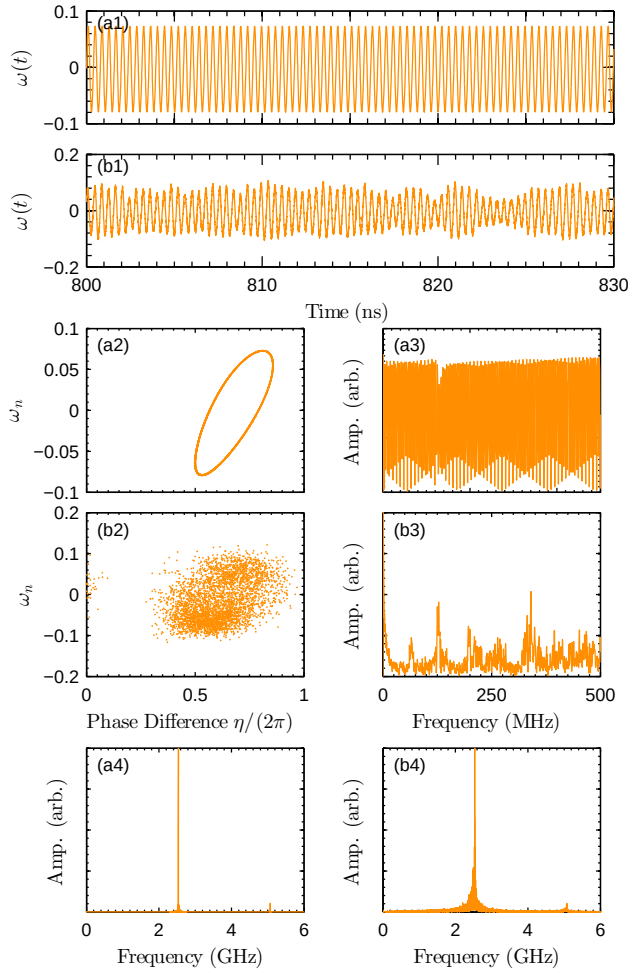

Figure 6: Deterministic (a) and stochastic (b) plots of the frequency $\omega(t)$ time-series (1), the phase-plane of ω_n and η (2), and the rf spectrum (3) when the feedback strength is κ_1 =0.97 GHz. The deterministic time-series and phase-portrait show periodic behavior with a frequency of $f_{RO} \approx 2.5$ GHz, which is shown in the extended spectra (a4) and (b4).

and filter bandwidth.

Turning our attention to the period doubling maps [Fig. 2], we note that the transition into chaotic deterministic dynamics begins at a feedback strength of $\kappa_1 \approx 4.5$ GHz (f_{IV} on the map), and in presence of noise the onset of a chaotic transition is clearly delayed ($\kappa_1 \approx 7.0$ GHz). Fig. 7 displays this critical transition at a feedback κ_1 =4.52 GHz for the deterministic onset of chaos. The frequency $\omega(t)$ not only oscillates with a period of $1/f_{RO}$ but exhibits an envelope of slower oscillations which are shown in the time series (a1) and spectrum (a2) of Fig. 7. The return map in Fig. 8(a) suggests stable periodic oscillations demonstrated by the small variance in the deterministic maximum values (blue circle) of the frequency ω_{max}. Comparing this to the stochastic dynamics, the corresponding behaviors are very different. Shown in Fig. 7(b2), the attractor no longer survives and the spectrum [Fig. 7(b3)] greatly differs. The spectrum contains a period doubled

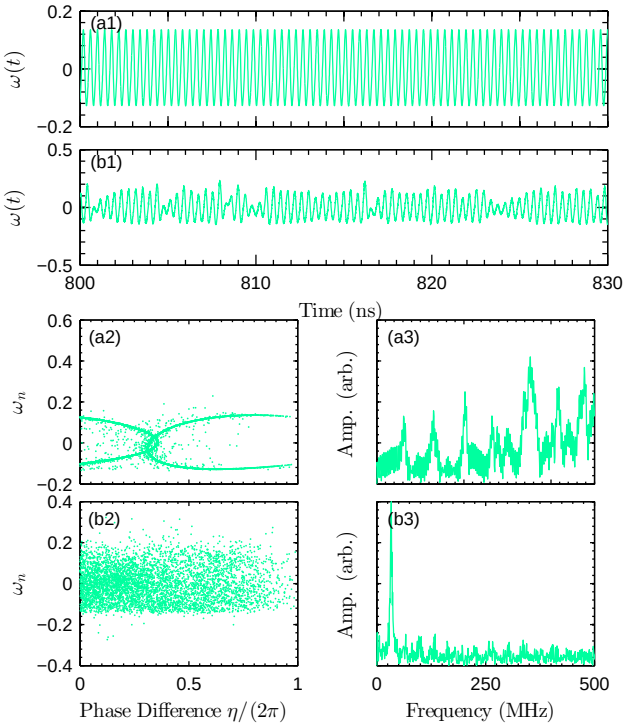

Figure 7: Deterministic (a) and stochastic (b) plots of the frequency $\omega(t)$ time-series (a1 and b1), the phase-plane of ω_n and η (a2 and b2), and the rf spectrum (a3 and b3) when the feedback strength is κ_1 =4.52 GHz.

frequency located at $f_{dom}/2$ = 62 MHz. Here we define f_{dom} as the dominant frequency which corresponds to the weighted average between the two fundamental frequencies of each cavity. Once again, the dominant frequency in the presence of noise is dictated by the FOF time scales (τ and Λ).

The return maps in Fig. 8 for feedback strengths κ_1 =4.84 GHz [Fig. 8(b)] and κ_1 =5.16 GHz [Fig. 8(c)] provide an excellent representation of the difference between the deterministic and stochastic dynamical states. Comparing all three return maps [Fig. 8a,b, and c], the stochastic maxima (red triangles) reveal a departure from the linear shape at smaller feedback strengths (see Fig. 5). The deterministic maxima (blue circles) ω_{max}, however, require a larger feedback strength (κ_1 =5.16 GHz) in order to replicate stochastic maps. It is not until κ_1 =5.16 GHz [Fig. 8(c)] that the two maps become similar.

However, the similarity in the return maps [Fig. 8(c)] does not guarantee that the dynamical states will be identical. The difference between the stochastic and deterministic dynamics is manifested in the period doubling routes shown in Fig. 2, where two key differences standout. First, the lack of stable RO frequencies in Fig. 2(b) (stochastic), which are present in Fig. 2(a) (deterministic). An example of the RO frequency in Fig. 2(a) is displayed by the marker f_{III}. Second, the onset of chaos is delayed in Fig. 2(b) until a feedback strength of $\kappa_1 \approx 7$ GHz is reached. To explain these differences, it appears that multiple mecha-

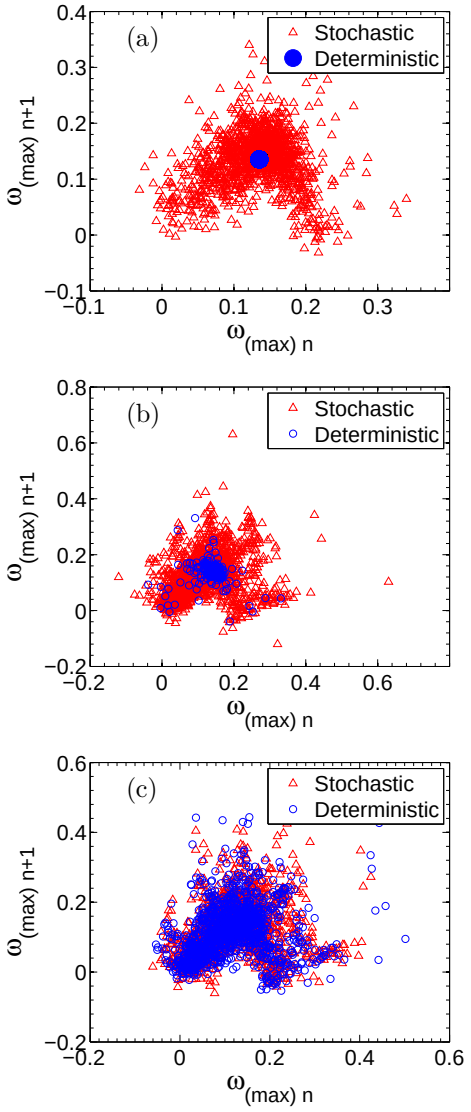

Figure 8: First return maps for feedback strength of (a) κ_1 =4.52 GHz, (b) κ_1 =4.84 GHz, and (c) κ_1 =5.16 GHz showing both the stochastic (red triangle) and deterministic (blue circle) values.

nisms play a role. Not only does noise limit the number of stable attractors, but noise drives the periodic oscillations toward the dynamics influenced by the time-delay and filter bandwidth.

4. Effects of the filter bandwidth on the dynamics

We next turn our attention to the effects of the two filter bandwidths on the dynamics. In a single FOF system, it is possible to identify three regimes depending on the magnitude of the bandwidth Λ relative to the RO frequency f_{RO} and relative to the external cavity mode (ECM) spacing. The effects of the filter width on the dynamics for each case have been outlined by Fischer [25], while other theoretical work has characterized the mode structures for the different bandwidth regimes [26]. Our previous bifurcation analysis was done for bandwidths of equal magnitudes, $\Lambda_1 = \Lambda_2 = 1$ GHz, which fall in an intermediate range. The intermediate range is where Λ is large enough to include a number of ECMs yet smaller than the frequency of the ROs. A narrow filter ($\Lambda \to 0$) was shown to resemble optical injection [27], while a wide filter ($\Lambda \to \infty$) was shown to resemble conventional optical feedback (COF), hence the latter case reduces to the standard Lang-Kobayashi rate equations [26]. In general, the most interesting dynamics occur in the intermediate regime, because in this regime the parameters of the filter (Λ and Δ) play an important role in determining both the stability and control of the dynamics [25].

The use of two filters is advantageous not only because of the additional parameters introduced (τ_2, Λ_2, Δ_2, *etc.*) but also because of the interplay between the two fields which results in novel dynamics and the possibility of robust control over these dynamics [18]. As stated earlier, we fix one filter Λ_1 in the intermediate regime while the other filter Λ_2 is varied. In particular, we focus on two cases. The first is a narrow filter $\Lambda_2 < \delta_{ECM}$, where δ_{ECM} is the frequency of the external cavity mode spacing. The second is a wide filter, $\Lambda_2 > f_{RO}$. We achieve this by varying the bandwidth of one filter over a large range from $\Lambda_2 = 0 \to 20$ GHz, while the second filter is fixed at $\Lambda_2 = 1$ GHz. We focus on these two cases in order to isolate the effects of both noise and the bandwidth. A study could be done of the narrow-narrow, wide-wide, or narrow-wide cases, but these would no longer contain any signatures of the spectrally filtered feedback. Rather, they would resemble injection and COF.

4.1. Feedback from an intermediate and narrow filter

In practice, one is not able to reduce the bandwidth indefinitely, therefore we restrict ourselves to the narrow filter where $0 < \Lambda < \delta_{ECM}$. Experimentally, the bandwidth of the filter can be modified by changing the mirror reflectivity of the filter or the mirror spacing. We study this system by keeping $\Lambda_2 = 1$ GHz while Λ_1 and Δ_1 are varied from 10 MHz to 50 MHz and -10 MHz to -50 MHz, respectively, where 50 MHz is slightly larger than the SCL linewidth. Along each iteration of the bandwidth, the detuning is varied such that the laser frequency lies at the same position of the filter profile. Similar to the period doubling map, the spectra are stitched together for different Λ_1 and Fig. 9 shows the resultant density plots of the intensities (1) $I_L(t)$, (2) $I_{F_1}(t)$, and (3) $I_{F_2}(t)$, where $I_L(t) = |E(t)|^2$, $I_{F_1}(t) = |F_1(t)|^2$, and $I_{F_2}(t) = |F_2(t)|^2$.

Initially, for the deterministic case, when Λ_1 is small (0 MHz $< \Lambda_1 <$ 20 MHz), the frequency of oscillations is $f_{dom} \approx 110$ MHz shown in Figure 9(a). This frequency of 110 MHz corresponds to the fundamental frequency of cavity 2. Using the parameters in Table 1, we find that $f_2 \approx 1/(\tau_2 + 1/\Lambda_2) \approx 112$ MHz. When Λ_1 is increased, a frequency of 50 MHz emerges, which is a consequence of the spectrally filtered feedback from cavity 1. The frequency of 50 MHz is an average between f_1 and f_2, where

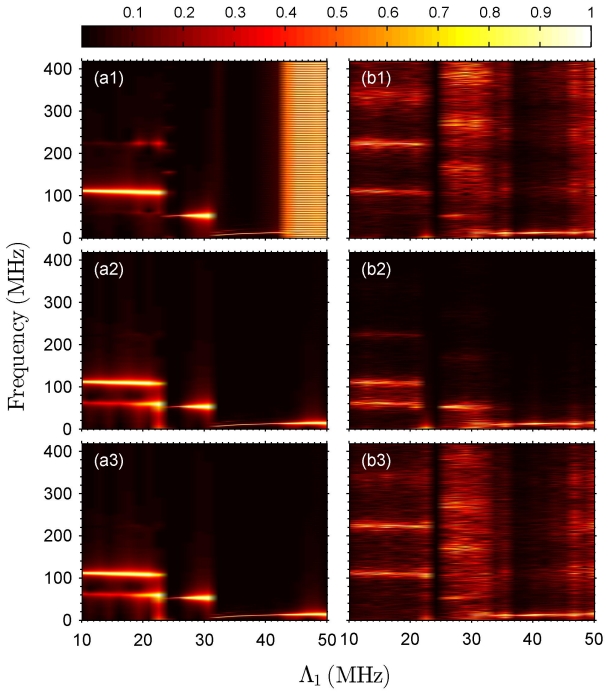

Figure 9: Deterministic (a) and stochastic (b) density plots of the amplitude of the spectrum as a function of changing bandwidth, Λ_1. The density plots correspond to the spectra for (1) $I_L(t)$, (2) $I_{F_1}(t)$, (3) and $I_{F_2}(t)$. Λ_2 is fixed at 1 GHz and the two feedback rates are kept constant at $\kappa_1 = 3$ GHZ and $\kappa_2 = 0.8$ GHz.

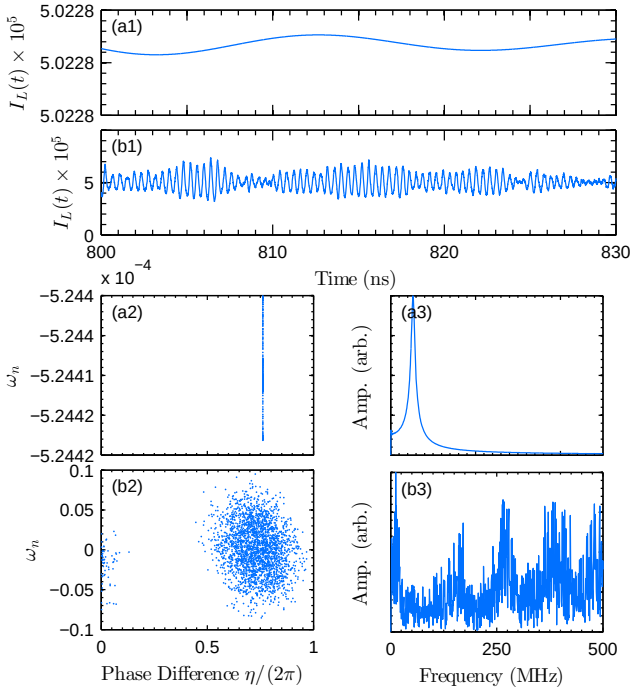

Figure 10: (1) Intensity time series $I_L(t)$, (2) phase portraits (η, P), and (3) rf spectrum in the absence of noise (a) and in the presence of noise (b) for a bandwidth of $\Lambda_1 \approx 32$ MHz and detuning $\Delta_1 = -32$ MHz.

$f_1 \approx 1/(\tau_1 + 1/\Lambda_1) \approx 15$ MHz. The average, weighted toward f_1, is explained by the larger feedback rate from cavity 1 ($\kappa_1 > \kappa_2$). The dependence of the weighted average on the ratio of the feedback rates was reported in Ref. [18]. Continuing to increase Λ_1 results in a frequency of approximately 15 MHz, which is dominated by f_1. Upon further increase of Λ_1 the ROs become dominant which is evident in the time series plot in Fig. 11(a1). Note that these ROs are not present in Figs. 9(a2) and 9(a3) because, Λ_1 and Λ_2 act as low pass filters. The same density plots are then produced in the presence of noise shown in Fig. 9b. For all three plots in Fig. 9b, there is an absence of the broad 50 MHz frequency at a bandwidth of $\Lambda_1 = 32$ MHz.

The deterministic time series for $\Lambda_1 = 32$ MHz in Fig. 10(a1) shows the evolution of $I_L(t)$ toward a steady-state value and the phase portrait (a2) shows this fixed point attractor. Comparing this to the stochastic time series for $\Lambda_1 = 32$ MHz in Fig. 10(b1), it becomes evident that noise drives the system out of the fixed point, which was explained in our analysis above describing the period-doubling route to chaos. Comparing Fig. 11(a1) and Fig. 11(b1), it is clear that the relaxation oscillations are no longer the dominant frequency for the deterministic case at a larger bandwidth of $\Lambda_1 = 50$ MHz, rather the dominant frequency contains signatures of the FOF time scale in the rf spectrum shown in Fig.11(b3).

Although $\Lambda_1 < \delta_{ECM}$, we point out that the feedback

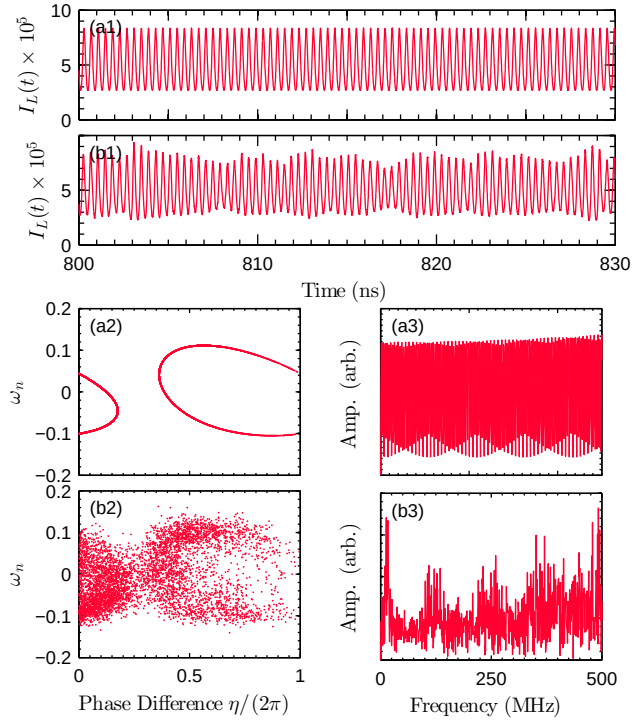

Figure 11: (1) Intensity time series $I_L(t)$, (2) phase portraits (ω_n, η), and (3) rf spectrum in the absence of noise (a) and in the presence of noise (b) for a bandwidth of $\Lambda_1 = 50$ MHz and detuning $\Delta_1 = -50$ MHz.

from cavity 1 only resembles optical injection when the bandwidth is $\Lambda_1 < 25$ MHz. This is observed by noting that the dynamics in the presence of cavity 1 alone, when $\kappa_2 = 0$ GHz (not shown), evolve to a steady-state fixed point for any bandwidth of Λ_1 up to 25 MHz. Beyond a bandwidth of $\Lambda_1 = 25$ MHz the dynamics become periodic and the period of these dynamics depend on the filter bandwidth, thus no longer considered optical injection. In summary, both the narrow-intermediate and intermediate-intermediate cases show that particular attractors no longer survive and, in turn, drive the system toward periodic oscillations determined by the a FOF time scales (τ and Λ). This relationship, however, is for two particular feedback rates κ_1 and κ_2. A complete picture becomes highly complex due to the amount of parameters $\Lambda_{1,2}, \tau_{1,2}, \Delta_{1,2}, \kappa_{1,2}$ which influence the dynamical behavior of this system.

4.2. Feedback from an intermediate and wide filter

We next investigate the effects of a competition between an intermediate filter and wide filter. The dynamics of both cases have been intensely studied for the single FOF case which showed that the stability and dynamics vary depending on the filter width [25]. Knowing that the wide filter resembles COF, we expect to see only two time signatures (τ and $1/f_{RO}$), instead of the influence of the bandwidth Λ found in FOF dynamics.

To study this system, we fix both bandwidths at $\Lambda_1 = 20$ GHz and $\Lambda_2 = 1$ GHz and detunings $\Delta_1 = -5$ GHz and $\Delta_2 = -1.5$ GHz. κ_1 is varied while $\kappa_2 = 0.8$ GHz is fixed. κ_1 is varied, rather than Λ_1, because the period of elicited oscillations for this two FOF system remain unaltered when Λ_1 is increased. Fig. 12 contains the spectra of the intensity of the laser $I_L(t)$ and the intensity of the light through filter 2, $I_{F_2}(t)$, when the feedback rate κ_1 is varied. These two intensities were chosen because the light through filter 1, I_{F_1}, directly mimics $I_L(t)$ due to the wide filter and the presence of the ROs, which are not as dominant in the dynamics of feedback from filter 2.

Initially, the feedback is solely from cavity 2 ($\kappa_1 = 0$ GHz). Therefore, the dynamics which arise are a consequence of the spectrally filtered (intermediate) feedback from cavity 2, which are shown in Fig. 13 for feedback rates of $\kappa_2 = 0.8$ GHz and $\kappa_1 = 0$ GHz. It is clear that the rf spectra of the deterministic (a3) and stochastic (b3) dynamics are very similar at this feedback strengths. The dominant frequency $f_2 \approx 112$ MHz corresponds to the fundamental frequency of cavity 2. The higher harmonics are also present with decreasing amplitudes. The feedback rate κ_1 is increased which enhances the second and third harmonic shown in both Fig. 12(a1) and (a2). As the feedback rate increases, $\kappa_1 \approx 0.32$ GHz, a frequency at $f \approx 66$ MHz emerges. We note that this corresponds to the fundamental frequency from cavity 1 which is $f_1 \approx 1/\tau_1$, which has no signatures of the bandwidth ($\Lambda_1 = 20$ GHz). A continued increase in κ_1 results in the enhancement of

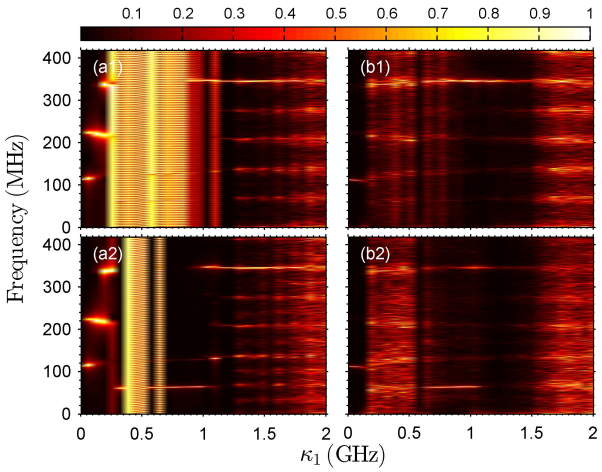

Figure 12: Deterministic (a) and stochastic (b) density plots of the amplitude of the spectrum as a function of the increasing feedback rate, κ_1. The spectra are calculated with the with the parameters mentioned in Table 1 except the following: $\Lambda_1 = 20$ GHz and $\Delta_1 = -5$ GHz. (1) Spectra of the intensity of light from laser, $I_L(t)$ and (2) spectra from the light through filter 2, $I_{F_2}(t)$.

the successive higher harmonics, the second and third harmonic emerge, $2f_1$ and $3f_1$ respectively. The ROs appear in the laser intensity, which is shown Fig.12(a1), while they are attenuated through filter 2 shown in Fig. 12(a2).

The dynamics become more complicated and eventually evolve into the chaotic regime as the feedback rate κ_1 is increased. This is seen in all three subplots in Fig. 13(c1) and Fig 13(d1) at feedback rate of $\kappa_1 = 1.7$ GHz. The complicated time series, the jumping between attractors in the phase portrait and the spread in the rf spectrum all indicate the emergence of a chaotic regime. This behavior is well known for COF systems as the feedback rate is increased eventually inducing coherence collapse.

Comparing the deterministic [Fig. 12(a)] and stochastic [Fig. 12(b)] spectra (density plots) for an increasing feedback strength (κ_1), it is evident that noise plays a significant role in determining which frequencies emerge. This is understood by noting that the filter widths are larger, thus effectively reducing the spectral filtering of the feedback fields. Initially, the frequency spectra are very similar when $\kappa_1 = 0$ GHz shown in Fig.13(a3) and Fig. 13(b3). As κ_1 is increased, two regions of dissimilarity emerge. The first is a lack of the second and third harmonic found in Fig. 12(b). Upon further investigation we found that these harmonics emerge as the system evolves toward a steady state intensity. When the feedback rate is 0.1 GHz $< \kappa_1 <$ 0.3 GHz, noise drives the system out of these fixed point solutions, which is in good agreement with the previous analysis.

However, it is interesting to note that noise does not appear to delay the onset of chaos in larger feedback regimes ($\kappa_1 > 1.5$ GHz) shown in Fig. 12(b). A stark difference between the former bandwidth regimes and the wide-intermediate regime is that there is no averaging between

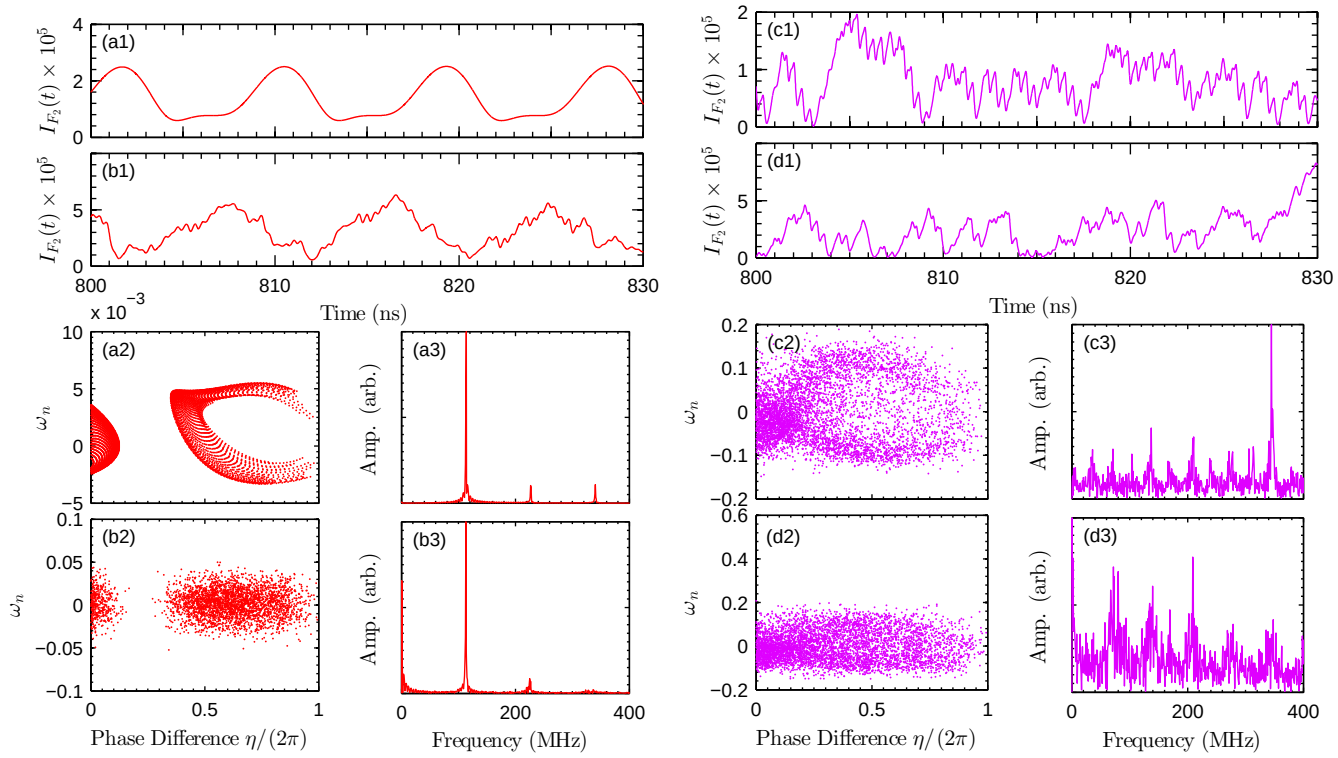

Figure 13: Three subplots are produced using the intensity of light through filter 2, $I_{F_2}(t)$. The times series (1), phase portrait $\omega_n, \eta(t)$ (2), and rf spectrum (3) are calculated for the feedback rates [(a) and (b)] $\kappa_1 = 0$ GHz and [(c) and (d)] $\kappa_1 = 1.7$ GHz.

the fundamental frequencies of the cavities, i.e. the dynamics are dictated by cavity 2 (intermediate filter) or cavity 1 (wide filter). In the presence of noise, two chaotic regimes emerge, when 0.3 GHz $< \kappa_1 <$ 0.55 GHz and $\kappa_1 > 1.7$ GHz [Fig. 12(b)]. For small feedback strengths (0.3 GHz $< \kappa_1 <$ 0.55 GHz) when the RO dynamics emerge [Fig. 12(a)], instead of driving the system toward periodic oscillations, the dynamics become chaotic [Fig. 12(b)]. In summary, the presence of a large bandwidth does not filter the frequency content and thus permits chaotic dynamics when the deterministic periodic (ROs) attractors no longer survive in the presence of noise even for a smaller feedback rate (0.3 GHz $< \kappa_1 <$ 0.55 GHz).

5. Discussion and conclusion

In this paper, we have reported on a theoretical and computational investigation of the effects of quantum noise on the complex dynamics that arise in the instantaneous optical frequency of a SCL that is subject to two filtered optical feedbacks. A majority of the results deal with the situation where the bandwidths of both filters through which the feedbacks are filtered are in the intermediate regime and wherein the feedback strength from one cavity is kept fixed while the feedback strength from the second cavity is varied. For these parameters, the most important observation is that the feedback strength needed from the second cavity to produce coherence collapse is significantly increased in the presence of noise. Our calculations indicate that this is a general feature of two FOFs in the presence of noise, even though we have displayed the results for one set of parameters. The physical origin of this increased feedback needed to produce coherence collapse lies in the fact that some of the attractors in the deterministic model do not survive in the presence of noise. An important consequence of this is that the effects of the time-delay and filter bandwidth are enhanced in the presence of quantum noise.

Most of the results that we report show the dynamics up to frequencies of a few hundred MHz since these can be easily measured with standard detection components with rise times of a few nanoseconds. In some representative cases we also show the observed behaviors extended out to a few GHz, and the dominant theme to emerge from these data is that as the feedback strength from the second cavity is increased, the relaxation oscillations become the more dominant feature. In general, the results indicate that the effect of noise is to destroy the periodic attractor related to the relaxation oscillations and to enhance the effects of time-delay and filter bandwidth.

Typically, the effects of quantum noise will be most prominent when both filters have bandwidths in the intermediate regime. For narrow filters, any relaxation oscillations that are undamped will be suppressed by the narrow filters and hence the dynamics will be dominated by the time-delay of the feedbacks. For wide filters, signatures

of the time-delayed feedback will be suppressed by the relaxation oscillations. It is only the intermediate regime in which noise can push the dynamics either towards making the time-delay dynamics the dominant ones or the relaxation oscillations the dominant ones, depending on feedback strengths.

This paper also reports the laser frequency dynamics when one of the filters has an intermediate bandwidth and the other is either much narrower or much wider. In the former case, the effect of quantum noise is to once again drive the system away from the deterministic fixed point. In addition, the relaxation oscillations are suppressed and the time scale associated with the time-delayed feedback and the filter bandwidth contribute to the dominant frequencies. In the case of one intermediate filter and one wide filter, the spectral filtering of the feedback is reduced and as a consequence one finds that the laser frequency goes into the coherence collapse regime at about the same feedback levels in the presence of quantum noise as it does in the deterministic case. Therefore, it is clear that the requirement for a higher feedback strength to induce coherence collapse in the presence of quantum noise arises only when the filter bandwidths are in the intermediate regime, even though noise does play a role in determining which deterministic attractors persist.

In summary, our work confirms that it is important to include the role of quantum noise to accurately describe the frequency dynamics of a SCL subject to two FOFs. The complexity and richness of this multi-parameter system raises some interesting and important questions, such as the physical mechanisms that cause laser frequency dynamics to be dominated by the time-delay and filter bandwidth in the two intermediate filter case, the reasons for the return maps to deviate from a linear shape in the presence of noise, the effects of correlated amplitude and inversion noise, and the influence of different noise strengths and of other combinations of filter widths. We hope to explore these, and other, questions in future studies.

6. Acknowledgments

This research was supported in part by Lilly Endowment, Inc., through its support for the Indiana University Pervasive Technology Institute, and in part by the Indiana METACyt Initiative. The Indiana METACyt Initiative at IU is also supported in part by Lilly Endowment, Inc.

References

[1] M. C. Soriano, J. García-Ojalvo, C. R. Mirasso, I. Fischer, Complex photonics: Dynamics and applications of delay-coupled semiconductors lasers, Rev. Mod. Phys. 85 (2013) 421–470. doi:10.1103/RevModPhys.85.421.
URL http://link.aps.org/doi/10.1103/RevModPhys.85.421

[2] M. Sciamanna, K. Shore, Physics and applications of laser diode chaos, Nature Photonics 9 (3) (2015) 151–162.

[3] M. C. Soriano, S. Ortín, D. Brunner, L. Larger, C. R. Mirasso, I. Fischer, L. Pesquera, Optoelectronic reservoir computing: tackling noise-induced performance degradation, Opt. Express 21 (1) (2013) 12–20. doi:10.1364/OE.21.000012.
URL http://www.opticsexpress.org/abstract.cfm?URI=oe-21-1-12

[4] M. Peil, M. Jacquot, Y. K. Chembo, L. Larger, T. Erneux, Routes to chaos and multiple time scale dynamics in broadband bandpass nonlinear delay electro-optic oscillators, Phys. Rev. E 79 (2009) 026208. doi:10.1103/PhysRevE.79.026208.
URL http://link.aps.org/doi/10.1103/PhysRevE.79.026208

[5] R. Lang, K. Kobayashi, External optical feedback effects on semiconductor injection laser properties, Quantum Electronics, IEEE Journal of 16 (3) (1980) 347–355. doi:10.1109/JQE.1980.1070479.

[6] D. Lenstra, B. Verbeek, A. Den Boef, Coherence collapse in single-mode semiconductor lasers due to optical feedback, Quantum Electronics, IEEE Journal of 21 (6) (1985) 674–679. doi:10.1109/JQE.1985.1072725.

[7] T. Heil, A. Uchida, P. Davis, T. Aida, Te-tm dynamics in a semiconductor laser subject to polarization-rotated optical feedback, Phys. Rev. A 68 (2003) 033811. doi:10.1103/PhysRevA.68.033811.
URL http://link.aps.org/doi/10.1103/PhysRevA.68.033811

[8] N. Oliver, M. C. Soriano, D. W. Sukow, I. Fischer, Dynamics of a semiconductor laser with polarization-rotated feedback and its utilization for random bit generation, Opt. Lett. 36 (23) (2011) 4632–4634. doi:10.1364/OL.36.004632.
URL http://ol.osa.org/abstract.cfm?URI=ol-36-23-4632

[9] G. Friart, G. Verschaffelt, J. Danckaert, T. Erneux, All-optical controlled switching between time-periodic square waves in diode lasers with delayed feedback, Opt. Lett. 39 (21) (2014) 6098–6101. doi:10.1364/OL.39.006098.
URL http://ol.osa.org/abstract.cfm?URI=ol-39-21-6098

[10] G. Friart, A. Gavrielides, T. Erneux, Analytical stability boundaries of an injected two-polarization semiconductor laser, Phys. Rev. E 91 (2015) 042918. doi:10.1103/PhysRevE.91.042918.
URL http://link.aps.org/doi/10.1103/PhysRevE.91.042918

[11] M. Yousefi, D. Lenstra, Dynamical behavior of a semiconductor laser with filtered external optical feedback, Quantum Electronics, IEEE Journal of 35 (6) (1999) 970–976. doi:10.1109/3.766841.

[12] A. P. A. Fischer, M. Yousefi, D. Lenstra, M. W. Carter, G. Vemuri, Filtered optical feedback induced frequency dynamics in semiconductor lasers, Phys. Rev. Lett. 92 (2004) 023901. doi:10.1103/PhysRevLett.92.023901.
URL http://link.aps.org/doi/10.1103/PhysRevLett.92.023901

[13] H. Erzgräber, B. Krauskopf, D. Lenstra, A. P. A. Fischer, G. Vemuri, Frequency versus relaxation oscillations in a semiconductor laser with coherent filtered optical feedback, Phys. Rev. E 73 (2006) 055201. doi:10.1103/PhysRevE.73.055201.
URL http://link.aps.org/doi/10.1103/PhysRevE.73.055201

[14] L. Jaurigue, E. Sch oll, K. L udge, Passively mode-locked laser coupled to two external feedback cavities (2015). doi:10.1117/12.2076118.
URL http://dx.doi.org/10.1117/12.2076118

[15] P. Slowiński, B. Krauskopf, S. Wieczorek, Mode structure of a semiconductor laser with feedback from two external filters, Discrete and Continuous Dynamical Systems - Series B 20 (2) (2015) 519–586. doi:10.3934/dcdsb.2015.20.519.
URL http://aimsciences.org/journals/displayArticlesnew.jsp?paperID=10722

[16] P. Slowiński, B. Krauskopf, S. Wieczorek, Mode structure of a semiconductor laser with feedback from two external filters (2008). doi:10.1117/12.780576.
URL http://dx.doi.org/10.1117/12.780576

[17] P. Slowiński, B. Krauskopf, S. Wieczorek, Solution structure and dynamics of a semiconductor laser subject to feedback from two external filters (2010). doi:10.1117/12.853448.
URL http://dx.doi.org/10.1117/12.853448

[18] V. Pal, J. Suelzer, A. Prasad, G. Vemuri, R. Ghosh, Semiconductor laser dynamics with two filtered optical feedbacks,

Quantum Electronics, IEEE Journal of 49 (3) (2013) 340–349. doi:10.1109/JQE.2013.2244559.

[19] G. Agrawal, N. Dutta, Long wavelength semiconductor lasers, Van Nostrand Reinhold Co. Inc.,New York, NY, 1986.

[20] G. Gray, R. Roy, Noise in nearly-single-mode semiconductor lasers, Phys. Rev. A 40 (1989) 2452–2462. doi:10.1103/PhysRevA.40.2452.
URL http://link.aps.org/doi/10.1103/PhysRevA.40.2452

[21] M. Yousefi, D. Lenstra, G. Vemuri, Nonlinear dynamics of a semiconductor laser with filtered optical feedback and the influence of noise, Phys. Rev. E 67 (2003) 046213. doi:10.1103/PhysRevE.67.046213.
URL http://link.aps.org/doi/10.1103/PhysRevE.67.046213

[22] R. L. Honeycutt, Stochastic runge-kutta algorithms. i. white noise, Phys. Rev. A 45 (1992) 600–603. doi:10.1103/PhysRevA.45.600.
URL http://link.aps.org/doi/10.1103/PhysRevA.45.600

[23] C. Masoller, Noise-induced resonance in delayed feedback systems, Phys. Rev. Lett. 88 (2002) 034102. doi:10.1103/PhysRevLett.88.034102.
URL http://link.aps.org/doi/10.1103/PhysRevLett.88.034102

[24] A. Hohl, A. Gavrielides, Bifurcation cascade in a semiconductor laser subject to optical feedback, Phys. Rev. Lett. 82 (1999) 1148–1151. doi:10.1103/PhysRevLett.82.1148.
URL http://link.aps.org/doi/10.1103/PhysRevLett.82.1148

[25] A. Fischer, M. Yousefi, D. Lenstra, M. Carter, G. Vemuri, Experimental and theoretical study of semiconductor laser dynamics due to filtered optical feedback, Selected Topics in Quantum Electronics, IEEE Journal of 10 (5) (2004) 944–954. doi:10.1109/JSTQE.2004.835997.

[26] H. Erzgräber, B. Krauskopf, Dynamics of a filtered-feedback laser: influence of the filter width, Opt. Lett. 32 (16) (2007) 2441–2443. doi:10.1364/OL.32.002441.
URL http://ol.osa.org/abstract.cfm?URI=ol-32-16-2441

[27] T. Erneux, G. Hek, M. Yousefi, D. Lenstra, The injection laser limit of lasers subject to optical feedback (2004). doi:10.1117/12.545898.
URL http://dx.doi.org/10.1117/12.545898